

Hyperon-nucleon interactions in the $pp \rightarrow K^+ \Lambda p$ reaction

N. G. Kelkar and B. K. Jain

*Nuclear Physics Division, Bhabha Atomic Research Centre, Mumbai 400 085,
India.*

Abstract

We present calculations of the invariant mass spectra of the Λp system for the exclusive $pp \rightarrow K^+ \Lambda p$ reaction with the aim of studying the final state interaction between the Λ -hyperon and the proton. The reaction is described within a meson exchange framework and the final state Λp interaction is incorporated through an off-shell t-matrix for the $\Lambda p \rightarrow \Lambda p$ scattering, constructed using the available hyperon-nucleon (YN) potentials. The cross sections are found to be sensitive to the type of YN potential used especially at the Λ and Σ production thresholds. Hence, data on this exclusive reaction, which can be used to constrain the YN potentials are desirable.

PACS numbers: 13.75.Ev, 25.40.-h, 24.10.Eq

Keywords: Hyperon nucleon interaction, Kaon production, Λp invariant mass spectrum, Proton proton collision

1 Introduction

A good knowledge of the hyperon-nucleon (YN) interaction is crucial for the understanding of a variety of phenomena ranging from low energy hypernuclear physics to the strangeness production in high energy heavy ion collisions. However, due to the non-availability of sufficient YN scattering data, the YN interaction is still quite unknown. Apart from a recent measurement of the differential cross sections for Σ^+p elastic scattering [1], only an almost three decades old total and differential cross section data on YN scattering from bubble chamber experiments [2] exist. Since the experiments with short-lived secondary beams of strange particles are difficult to perform, reactions like the $K^-d \rightarrow \pi^-YN$ and $\pi^+d \rightarrow K^+YN$, involving the production of a YN pair in the final state, have received much attention [3]. Additionally, in the recent past, cross sections for the $pp \rightarrow K^+YN$ reaction have been measured [4, 5] at the Saturne National Laboratories for proton beam energies of 2.3 and 2.7 GeV and at COSY for proton energies very near to the threshold [6, 7]. Compared to the kaon and pion induced reactions, the $pp \rightarrow K^+YN$ reaction has the advantage that (i) the proton beams are easily available and (ii) the data are free from uncertainties due to the deuteron target as one can use a proton for the target nucleus.

Over the past few years, several theoretical models using different approaches (see ref.[8] for a detailed review) like the resonance model [9] and meson exchange model of Laget [10] have tried to explain the total cross section data [6, 11, 12] as well as the missing mass spectra of ref.[5] on the $pp \rightarrow K^+YN$ reaction. The calculation of the missing mass spectra by Deloff [13] using two different models of YN forces included only the ‘direct kaon emission’ (DKE) diagram and achieved qualitative agreement with data. Laget’s calculation involved a $(\pi + K)$ exchange mechanism in addition to DKE. With the cut-off mass Λ_K in the off-shell form factor for the exchanged kaon and the coupling constants $g_{N\Lambda K}$ and $g_{N\Sigma K}$ as free parameters, this model achieved good quantitative agreement with data.

However, the above analyses either neglect the final-state interaction between the Λp pair [8, 9] or use phenomenological prescriptions for the off-shell YN amplitudes. These approaches do not address the sensitivity of the cross sections to the specific description of the hyperon-nucleon potential $V_{\Lambda p}$. Due to the large momentum transfer involved in the $pp \rightarrow K^+\Lambda p$ reaction, we believe that the cross sections for this reaction should be sensitive to the details of the Λp potential. In a recent study of the weak strangeness producing reaction $pn \rightarrow p\Lambda$ [14] it was indeed found that apart from the weak transition potential the cross sections are very sensitive to the type of YN potential used. However, the cross sections for the weak reactions are very small ($\sim 10^{-12}$ mb). Hence the $pp \rightarrow K^+\Lambda p$ reaction which is experimentally feasible is a better choice for the study of the Λp interaction.

Currently there exist meson exchange models of V_{YN} which are similar in construction to the models of the well-known nucleon-nucleon (NN) interaction. The prominent ones among these are the Nijmegen and Jülich potentials [15, 16, 17, 18]. The free model parameters of the YN interaction in these models are fixed using the cross section data [2] on YN scattering. In addition to the meson exchange models, attempts to study the YN interaction using quark models have also been made

[19, 20, 21]. The V_{YN} in these models are constructed either using the resonating group method (RGM) or the quark cluster model approach. In the RGM [20], the total quark hamiltonian used consists of a confining piece, one gluon exchange potential and a chiral field induced quark-quark potential. The calculated YN phase shifts in this approach are found similar to those due to Nijmegen model F. The cluster model approach focuses mainly on the YN interactions at short distances and explores their characteristics from the spin and flavour symmetry structure, using one-gluon-exchange and the confining potential for the quark hamiltonian. In our work we use the boson-exchange models.

The aim of the present work is to study the sensitivity of the missing mass spectra in the $pp \rightarrow K^+\Lambda p$ reaction to V_{YN} , using as complete a description of the reaction as possible. We describe the Λp wave function in the final state by using the solution of the Lippmann-Schwinger equation. The t-matrix for the $\Lambda p \rightarrow \Lambda p$ scattering in this equation is constructed using the Nijmegen soft-core [15] and Jülich [18] potentials. This t-matrix includes the intermediate Σ state and hence the Λp wave function generated by us includes the effect of the ΣN channel on the Λp scattering.

As for the reaction mechanism, guided by the earlier investigations of the $pp \rightarrow K^+\Lambda p$ reaction using π and K exchange models [8, 10], we assume that it proceeds by the exchange of a pion or a kaon between the two protons in the entrance channel and neglect any contributions from heavier mesons like the ρ and K^* . In the case of π exchange, one of the interacting protons can be excited by the exchanged pion to any of the relevant N^* resonances, which then decays to a K^+ and Λ . In the case of kaon exchange, the K^+ and Λ are produced directly. In addition to these meson exchange diagrams, we also include the DKE diagram, where the proton in the initial state dissociates into K^+ and an off-shell Λ , which by its interaction with the second proton is brought on-shell. However its contribution is expected to be small because the intermediate Λ is *far* off-shell.

In our work we have included all the production diagrams shown in Fig. 1. Since it is not possible to fix the relative sign between the amplitudes corresponding to the pion and kaon exchange diagrams we choose to retain an additive sign between these amplitudes. The diagrams arising due to antisymmetrization of the two protons in the initial state have also been included. The amplitudes for $\pi^0 p \rightarrow K^+\Lambda$ and $K^+p \rightarrow K^+p$ at the kaon production vertices are constructed from the existing experimental data. Since these amplitudes fit the experimental data, they implicitly include the excitation of the resonances in πp scattering. The off-shell extrapolation is incorporated through a form factor.

In section 2 we describe the formalism used to evaluate the transition amplitude for the $pp \rightarrow K^+\Lambda p$ reaction. In section 3 we give the results. Experimental data on the missing mass spectra of the exclusive $pp \rightarrow K^+\Lambda p$ reaction do not exist. Hence we compare our results with the inclusive data of ref.[4] on the $pp \rightarrow K^+YN$ reaction. Upto the Σ threshold these data correspond only to the missing mass spectra for the $pp \rightarrow K^+\Lambda p$ reaction. However, above the Σ threshold, the contributions from the $pp \rightarrow K^+\Sigma N$ channels take over. The magnitude and shape of our calculated Λp mass spectra for the $pp \rightarrow K^+\Lambda p$ reaction are found to be sensitive to the type of Λp potential used. When compared with the inclusive data in the region below the Σ threshold, they are in reasonable agreement with the data. However, the

extent of agreement depends on the type of Λp potential used. At the opening of the Σ threshold, results with the Jülich potentials show a pronounced peak which appears only as a small kink in the case of the Nijmegen potential. For a more stringent constraint on the YN potentials, exclusive data on the various channels in the $pp \rightarrow K^+YN$ reaction are required.

In addition to the study of the Λp interaction we have also studied some other aspects of the $pp \rightarrow K^+\Lambda p$ reaction. Instead of using the detailed description for the Λp final state interaction as done in the present paper, it is always tempting to approximate it by an on-shell t-matrix multiplied by an off-shell extrapolating form factor, as done in ref. [10]. We have investigated the extent of accuracy of such a procedure by comparing the off-shell t-matrix computed by us with the corresponding on-shell t-matrix multiplied by an off-shell form factor. A detailed discussion of these results and those on the relative contributions of the various diagrams of Fig. 1 are given in section 3. Finally in section 4 we give a summary of this work.

Though this work has the limited plan of studying the $pp \rightarrow K^+\Lambda p$ reaction, we plan to extend our calculations to calculate the cross sections for the Σ producing channels too in future.

2 Formalism

The differential cross section for the reaction $p + p \rightarrow K^+ + p + \Lambda$ is given as [22],

$$d\sigma = \frac{1}{F} \int \frac{d\vec{p}_K}{2E_K} \frac{d\vec{p}_3}{2E_3} \frac{d\vec{p}_\Lambda}{2E_\Lambda} \delta(P_i - P_f) \left\langle \left| T_{fi} \right|^2 \right\rangle \quad (1)$$

where F is the *flux factor* and the angular brackets around $|T_{fi}|^2$ denote the average and sum over the spins of the particles in the initial and final states respectively. The momenta and energies of the two protons in the initial state and the K^+ , Λ and proton in the final state are denoted respectively as, $\vec{p}_1, \vec{p}_2, \vec{p}_K, \vec{p}_\Lambda, \vec{p}_3$ and $E_1, E_2, E_K, E_\Lambda, E_3$. Expressing the phase space integral in the above equation in terms of variables in the Λp centre of mass system (CMS), the double differential cross section is given as,

$$\frac{d^2\sigma}{d\Omega_K dW} = [PS] \times \int d\Omega_\Lambda^{(\Lambda p)} \left\langle \left| T_{fi} \right|^2 \right\rangle \quad (2)$$

where Ω_K is the laboratory solid angle of the emitted K^+ . W is the invariant mass of the Λp pair. $\Omega_\Lambda^{(\Lambda p)}$ is the solid angle of the Λ in the Λp CMS and PS is the phase space factor. All the kinematics is done relativistically.

T_{fi} , within a meson exchange framework (Fig. 1) consists of,

$$T_{fi} = T_K + T_\pi + T_{DKE} \quad (3)$$

where T_K and T_π correspond to the amplitudes of the kaon and pion exchange diagrams of Figs. 1a and 1b and T_{DKE} is the amplitude for direct K^+ emission as shown in Fig. 1c. The DKE by the proton leads to the formation of an off-shell Λ which is brought on-shell only after interacting with the second proton.

In what follows, we shall describe the various ingredients required for evaluating T_{fi} . Detailed expressions using partial wave expansions for the t-matrices being lengthy, are given in the appendix.

A. Final state interaction

Each of the T-matrices in eq.(3), which includes the interaction between the Λ and proton, is given by,

$$T_x = \left\langle \Psi_{\Lambda p}^- \vec{p}_K m_\Lambda m_3 \left| V_{pp \rightarrow K+\Lambda p}^x \right| \vec{p}_1 \vec{p}_2 m_1 m_2 \right\rangle - \text{exchange term} \quad (4)$$

where x is π , K or DKE. m_1 , m_2 , m_Λ and m_3 are the spin projections of the two entrance channel protons and the final state Λ and proton respectively. The exchange term arises due to the antisymmetrization of the two entrance channel protons and is written by interchanging \vec{p}_1 , m_1 with \vec{p}_2 , m_2 in the first term of the above equation. The final state Λp wave function $\Psi_{\Lambda p}^{-*}$ consists of a plane wave and a scattered wave and can be written as,

$$\Psi_{\Lambda p}^{-*} = \left\langle \vec{p}_\Lambda \vec{p}_3 \right| + \Psi_{scat}^* \quad (5)$$

where Ψ_{scat}^* is given in terms of the t-matrix for Λp scattering as,

$$\Psi_{scat}^* = \left\langle \vec{p}_\Lambda \vec{p}_3 \right| t_{\Lambda p \rightarrow \Lambda p} G_o. \quad (6)$$

Here G_o is the plane wave propagator for the Λp system in the intermediate state. Since the Λp momentum in this state is not fixed, the matrix $t_{\Lambda p \rightarrow \Lambda p}$ in the above expression is necessarily off-shell. The phase shift approximation to Ψ_{scat}^* is obtained by taking this t-matrix on-shell. In r-space this implies approximating the scattered wave function by its asymptotic form.

To obtain Ψ_{scat}^* , we consider the ΛN as well as the ΣN channels together. Ψ_{scat}^* is thus obtained by solving,

$$t_{\Lambda p \rightarrow \Lambda p} = V_{\Lambda p \rightarrow \Lambda p} + \left\langle \Lambda p \left| V G t \right| \Lambda p \right\rangle \quad (7)$$

where V , G and t are (2×2) matrices. G is the free Λp or ΣN propagator between two scatterings. The diagonal matrix elements describe respectively the $\Lambda p \rightarrow \Lambda p$ and $\Sigma N \rightarrow \Sigma N$ channels while the off-diagonal elements give the $\Lambda p \rightarrow \Sigma N$ and $\Sigma N \rightarrow \Lambda p$ transitions. Thus the constructed $t_{\Lambda p}$ includes the effect of the ΣN channel in Λp scattering. We construct $t_{\Lambda p}$ using the Nijmegen soft-core [15] and Jülich [18] YN potentials. We present results with both, the energy dependent versions (A, B) and energy independent versions (\tilde{A} , \tilde{B}) of the Jülich potential. The Nijmegen and Jülich models A and \tilde{A} are single meson exchange models whereas the Jülich models B and \tilde{B} involve higher order processes involving the intermediate Δ and Y^* . Both the Nijmegen and Jülich models provide a similar description of the YN total cross section data. However, there are significant differences in the inputs of these models. They differ in the choice of meson parameters, the contribution of

the various mesons to the YN interaction, their spin structure and in the treatment of non-localities. A detailed comparison of the various YN models can be found in refs. [18, 23].

B. Born amplitude $V_{pp \rightarrow K^+\Lambda p}^x$

The Born amplitude $V_{pp \rightarrow K^+\Lambda p}^x$ of eq. (4) is constructed using the kaon and pion exchange diagrams of Figs. 1a and 1b and the direct kaon emission (DKE) diagram in Fig. 1c. The DKE requires the Lagrangian for the $pK^+\Lambda$ vertex, which for the pseudoscalar coupling is given by,

$$\mathcal{L}_{pK^+\Lambda} = i g_{K\Lambda N} \bar{\Psi}_\Lambda \gamma_5 \Psi_p \vec{\tau} \cdot \vec{\phi}_K \quad (8)$$

where $\vec{\tau}$ is an isospin operator at the $pK^+\Lambda$ vertex. The expectation value of this Lagrangian over p and Λ wave functions is

$$\begin{aligned} \left\langle \vec{q}_\Lambda, \Lambda \left| \mathcal{L}_{pK^+\Lambda} \right| p, \vec{p}_1 \right\rangle &= i g_{K\Lambda N} \left[\frac{(E_1 + M_p)(E_\Lambda + M_\Lambda)}{2 M_p 2 M_\Lambda} \right]^{\frac{1}{2}} \\ &\times \left\langle \Lambda \left| \vec{\sigma} \cdot \left[\frac{\vec{p}_1}{E_1 + M_p} - \frac{\vec{q}_\Lambda}{E_\Lambda + M_\Lambda} \right] \right| p \right\rangle \vec{\tau} \cdot \vec{\phi}_K \end{aligned} \quad (9)$$

In addition to $\mathcal{L}_{pK^+\Lambda}$, the kaon exchange diagram involves the elastic scattering $K^+p \rightarrow K^+p$ of an off-shell kaon on a proton. A useful approximation to this amplitude which includes most of the dynamics at the scattering vertex, is to use a scattering amplitude determined phenomenologically from K^+p elastic scattering and corrected for the off-shell extrapolation by a form factor, $F_K(q_K^2)$ where q_K is the momentum carried by the off-shell kaon. For our calculations we take the scattering amplitude from ref. [24] and use the monopole form, $F_K(q_K^2) = (\Lambda_K^2 - M_K^2)/(\Lambda_K^2 - q_K^2)$ for the form factor.

For the pion exchange diagram we need the Lagrangian $\mathcal{L}_{\pi NN}$ and the amplitude for the $\pi^0 p \rightarrow K^+\Lambda$ process. Like in the case of $\mathcal{L}_{pK^+\Lambda}$ we use the pseudoscalar coupling for $\mathcal{L}_{\pi NN}$. The on-shell matrix elements for $\pi^0 p \rightarrow K^+\Lambda$ are related to those for the $\pi^- p \rightarrow K^0\Lambda$ reaction (for which the experimental data is available) due to isospin symmetry. We use the partial wave amplitudes given in ref.[25] which were constructed from all available experimental data on $\pi^- p \rightarrow K^0\Lambda$. The off-shell correction to this amplitude is again made using a monopole form factor, $F_\pi(q_\pi^2)$ where q_π is the momentum carried by the off-shell pion.

In order to describe consistently the Born transition amplitude $V_{pp \rightarrow K^+\Lambda p}^x$ and the Λp potentials which we use for the final state interaction, we take the values of the coupling constants and cut-off masses in the transition amplitude identical to those used in the construction of the Λp potentials [18]. The values of $g_{K\Lambda N}$ and $g_{\pi NN}$ are taken to be -14.1 and 13.3 respectively. The cut-off masses Λ_K and Λ_π in the monopole form factors $F_K(q_K^2)$ and $F_\pi(q_\pi^2)$ are taken to be 1.2 and 1.3 GeV respectively.

All our calculations are done using the partial wave expansion at every stage (see appendix for detailed expressions). Thus from the calculation point of view, our results are exact and carry all the details of the final state interaction and the amplitude $V_{pp \rightarrow K^+\Lambda p}^x$.

In this work we do not include the contribution to the $pp \rightarrow K^+\Lambda p$ reaction from the two step process which initially involves the excitation of a proton in the entrance channel to Σ and then its conversion to Λ through $\Sigma N \rightarrow \Lambda N$. The cross section for this process was found to be very small in the calculation of Ref. [10]. It was also found to be negligible in Ref. [26] where the authors studied the weak production of the Λ using a coupled channel approach for the Λp final state interaction. However, in a recent calculation [27] of the total cross sections for the $pp \rightarrow K^+\Lambda p$ reaction near threshold, a rather large contribution of this process was reported. In view of the results of Refs. [10, 26] and considering the smallness of the coupling constant involved at the $N\Sigma K$ vertex as compared to that at the $N\Lambda K$ vertex, we do not expect a significant contribution from the above mentioned process.

3 Results and Discussion

The main objective of our calculations is to study the effect of the final state interaction between the proton and Λ in the $pp \rightarrow K^+\Lambda p$ reaction and make an inter comparison of the calculated cross sections using the different available models of the hyperon-nucleon (YN) interaction. The differences in the various models of the YN interaction are expected to show up in the Λp invariant mass spectra because they involve Λp at different relative momenta starting from zero at threshold. These spectra should therefore be sensitive to the differences in the contributions of the various partial waves in different potentials for the Λp scattering and to the opening of the Σ production channel where the ${}^3S_1 - {}^3D_1$ coupled channels are important.

In Fig. 2 we show the differential cross section $d^2\sigma/d\Omega_K dW$ as a function of the invariant mass W of the Λp pair. Ω_K is the solid angle of the emitted kaon in the laboratory system. The proton beam energy is 2.3 GeV and the kaon angle is fixed at 10° . The thick solid line in Fig. 2a is our full calculation for the $pp \rightarrow K^+\Lambda p$ reaction with the Nijmegen potential for the Λp interaction. By ‘full’ we mean that the calculation includes all diagrams of Fig. 1, namely π plus K exchange and K^+ direct emission. The dash-dotted and dashed lines are respectively the full calculations with the energy independent versions \tilde{A} and \tilde{B} of the Jülich potentials. The thin solid line is the calculation using plane waves for the Λ and proton. In Fig. 2b we show the calculations using the energy dependent versions A and B of the Jülich potentials. We observe that all the curves with the Λp interaction included show an enhancement of the cross sections over the plane wave results, along the entire mass spectrum. The extent of the enhancement and the detailed structure in the spectrum, however, depend upon the choice of V_{YN} .

We now discuss the structures appearing in the Λp invariant mass spectra. As can be seen in Fig. 2a, the Jülich potential \tilde{A} produces a prominent cusp at the Σ threshold which is less prominent in the case of the Nijmegen potential. A rounded peak in the cross section at the Σ threshold is produced by the Jülich potential \tilde{B} . This peak is shifted in position as compared to the cusps. Similarly, at the Λ threshold we see sharp peaks or bumps in Figs. 2a and 2b, depending on the type of potential used. The shapes of these structures at the Λ and Σ thresholds, as shown recently in Ref. [28], are related to the location of the YN t-matrix poles in the various partial waves. The locations of these poles themselves, depend on

the details of the YN potential used. All the above mentioned potentials differ in their weightage of the different partial waves, though they have been constructed by fitting to the same set of ΛN elastic scattering data.

Next, we discuss the individual contributions of the various partial waves to the cross sections. Since the S waves are the most dominant in $\Lambda p \rightarrow \Lambda p$ scattering, in Fig. 3 we show the cross sections obtained by omitting the interactions in the S wave channels and the coupling between the 3S_1 and 3D_1 channel. The calculations are done using all the diagrams of Fig. 1 and two types of hyperon-nucleon potentials, namely the Nijmegen and the Jülich \tilde{A} . The thin solid line is the plane wave calculation in which the final state interaction of the Λ and proton is switched off completely. As can be seen in the figure, in the case of the Nijmegen Λp potential, removal of the interaction in the ${}^3S_1 - {}^3S_1$ channel brings down the cross sections (see dashed line) almost to the plane wave results. Omitting the ${}^3S_1 - {}^3D_1$ and ${}^3D_1 - {}^3S_1$ transitions in $\Lambda p \rightarrow \Lambda p$ scattering (dash-dotted line) has a small effect and the removal of the ${}^1S_0 - {}^1S_0$ channel causes a negligible change in the cross sections and cannot be seen in the figure. The Jülich potential however has its strength distributed more evenly over the various channels. The ${}^1S_0 - {}^1S_0$ transition specifically in this potential seems to be responsible for the peak at the Λ threshold.

Let us now see how the calculated cross sections using the various Λp potentials compare with the available data. In Fig. 4 we compare our calculated cross sections with the inclusive data of ref.[4] on the $pp \rightarrow K^+YN$ reaction, since there is no exclusive data available on the missing mass spectra in the $pp \rightarrow K^+\Lambda p$ reaction. Below the threshold for the Σ production ($W = 2128$ MeV) the data correspond entirely to that for the $pp \rightarrow K^+\Lambda p$ reaction. The steep rise in the measured cross sections at the Σ threshold is due to the opening of the Σ producing channels $pp \rightarrow K^+\Sigma^0 p$ and $pp \rightarrow K^+\Sigma^+ n$. We see that, while both the Nijmegen and Jülich potentials give the general trend of the data below the Σ threshold, in details they compare differently. The cross sections calculated using Jülich \tilde{A} agree somewhat with data at the Λ threshold. The peak at the Σ threshold is more pronounced with the Jülich potentials than with the Nijmegen potential. To constrain the YN potentials further, we need exclusive data on the Λp and ΣN channels.

Next, we investigate the accuracy of the on-shell approximation to the Λp final state interaction. For this we use the Nijmegen YN potential. In Fig. 5, the thick solid line is our calculation with the off-shell Λp t-matrix as in Fig. 2. The thin solid line is obtained by replacing the off-shell matrix elements $\langle JM(LS)p_{\Lambda p} | t^{\Lambda p \rightarrow \Lambda p} | q(L'S') JM \rangle$ in our calculations by the on-shell ones $\langle JM(LS)p_{\Lambda p} | t^{\Lambda p \rightarrow \Lambda p} | p_{\Lambda p}(LS) JM \rangle$. The scale for this curve is indicated on the right hand side of the figure. The scale for all other curves is indicated on the left. We see that the on-shell approximation results are much larger in magnitude and different in shape compared to those due to the correct t-matrix. This difference, however, is reduced to a great extent by multiplying the on-shell t-matrix by an off-shell form factor. The results obtained by repeating the same on-shell calculation with the above t-matrix elements multiplied by a form factor $F_{\Lambda p} = (p_{\Lambda p}^2 + \beta^2)/(q^2 + \beta^2)$ as in ref.[10] with $\beta = 1.36 fm^{-1}$ are shown by the dashed curve of Fig. 2. The form factor causes a large reduction of the cross sections and the pronounced peak at the Λ threshold flattens out. Still a considerable difference between this prescrip-

tion and the correct calculation persists. This difference can now be reduced and the calculated “on-shell” results can be brought nearer to the experimental measurement, by arbitrarily adjusting the parameters in the reaction vertices for the $pp \rightarrow K^+\Lambda p$ transition. The dash-dotted curve in Fig. 2 which agrees with data is the result for Λ_π , Λ_K and $g_{KN\Lambda}$ equal to 1.1 GeV, 0.925 GeV and -13.26 respectively. However, this way of constraining the transition amplitude parameters is obviously misleading.

So far we have discussed the results using the reaction mechanism involving all the diagrams of Fig. 1. Let us now see the contributions of the individual diagrams with the pion and kaon exchange and direct K^+ emission. In Fig. 6 we plot the cross sections with only pion exchange (dashed curves), only kaon exchange (dash-dotted curves) and the full calculation with π plus K exchange and K^+ direct emission (solid curves) for the Nijmegen and Jülich \tilde{A} Λp interactions. The contribution of the direct K^+ emission diagram is found to be negligibly small. The contribution of the kaon exchange diagram is much larger than that of the pion exchange diagram but it does not account completely for the cross sections. The dominance of the kaon-exchange diagram found here is consistent with some recent results reported by the DISTO Collaboration [29]. They performed a measurement of the polarization transfer coefficient D_{NN} for the $\vec{p}p \rightarrow pK^+\vec{\Lambda}$ reaction and found it to be very large and negative which is consistent with a mechanism dominated by kaon-exchange. In the next section we summarize the findings of this work.

4 Summary

We have studied the hyperon-nucleon (YN) final state interactions (FSI) in the $pp \rightarrow K^+\Lambda p$ reaction at 2.3 GeV beam energy. The invariant Λp mass spectra are calculated within a meson exchange framework. The FSI between the Λ and the proton are incorporated through a t-matrix for $\Lambda p \rightarrow \Lambda p$ scattering. This t-matrix is constructed using the Nijmegen and Jülich YN potentials. Due to unavailability of data on the invariant mass spectra in the exclusive $pp \rightarrow K^+\Lambda p$ reaction we compare our results with data on the inclusive $pp \rightarrow K^+YN$ reaction. Upto the Σ threshold the inclusive data receives contribution only from the exclusive $pp \rightarrow K^+\Lambda p$ channel.

The cross sections with FSI included are found to be enhanced compared to the plane wave results for both the potentials. However, the magnitude of the cross sections and the structure in them differ a lot for the two potentials. The general trend of the experimental data is produced by these calculations but in details they compare differently with data. Thus the exclusive data on the $pp \rightarrow K^+\Lambda p$ reaction can be very useful to differentiate amongst different V_{YN} .

Regarding the reaction mechanism involved, we find that the kaon exchange diagram gives the dominant contribution to the cross sections. This is consistent with some recent measurements of D_{NN} for the $\vec{p}p \rightarrow pK^+\vec{\Lambda}$ reaction made by the DISTO collaboration.

We have made a comparison of our results with the off-shell t-matrix for $\Lambda p \rightarrow \Lambda p$ scattering with those using the on-shell t-matrix. The on-shell results (even after multiplying by the off-shell form factor) overestimate the results obtained using the off-shell Λp t-matrix. Therefore, attempts to represent the FSI between the Λ and

proton by phase shifts (with an off shell form factor) may not represent the FSI accurately. This can lead to errors in conclusions about the parameters associated with the $pp \rightarrow K^+ \Lambda p$ transition interaction, if the same are adjusted to fit the data in this approach.

The present work can be improved by taking into account the actual off-shell nature of the $KN \rightarrow KN$ and $\pi N \rightarrow K\Lambda$ T-matrices. The final state $K\Lambda$ interaction may not be as small as that expected for the KN pair. It is incorporated in some sense in the pion exchange terms of the cross sections in this work since we use $T_{\pi N \rightarrow K\Lambda}$ constructed from experimental data. However it needs to be included explicitly in the kaon-exchange terms too. A calculation of the total cross sections and polarization observables with the $K\Lambda$ interaction included is planned for the future.

ACKNOWLEDGEMENTS

The authors wish to thank Angels Ramos for computational help related to the $\Lambda p \rightarrow \Lambda p$ t-matrix and for some useful discussions.

APPENDIX: TRANSITION AMPLITUDE FOR $pp \rightarrow K^+\Lambda p$

Let us start by writing the transition amplitude for the direct terms using the various diagrams shown in Fig. 1. The amplitudes for the exchange terms arising due to the antisymmetrization of the two initial protons are written by interchanging \vec{p}_1, E_1, m_1 with \vec{p}_2, E_2, m_2 in the equations to follow. In a distorted wave Born approximation the transition amplitude for the $pp \rightarrow K^+\Lambda p$ reaction is given as,

$$T_x = \sum_{SM_S} \left\langle \frac{1}{2} \frac{1}{2} m_3 m_\Lambda \left| S M_S \right. \right\rangle \left\langle p_{\vec{K}} \Psi_{p_{\vec{\Lambda}p} S M_S}^- \left| V_{pp \rightarrow K^+\Lambda p}^x \left| p_1 \vec{p}_2 m_1 m_2 \right. \right. \right\rangle \quad (\text{A.1})$$

where x is either π, K or DKE corresponding to pion and kaon exchange and direct K^+ emission as shown in Fig. 1 and $p_{\vec{\Lambda}p}$ is the momentum of the Λ and proton in the Λp centre of mass system. $\Psi_{p_{\vec{\Lambda}p} S M_S}^-$ is the distorted relative wave function for the Λp pair in the final state. $\langle p_{\vec{K}} |$ is the relative plane wave of K^+ with respect to the centre of mass of the Λp system. Now using the Lippmann-Schwinger equation for $\Psi_{p_{\vec{\Lambda}p} S M_S}^-$ we get,

$$T_x = \sum_{SM_S} \left\langle \frac{1}{2} \frac{1}{2} m_3 m_\Lambda \left| S M_S \right. \right\rangle \left[\left\langle p_{\vec{K}} p_{\vec{\Lambda}p} S M_S \left| V_{pp \rightarrow K^+\Lambda p}^x \left| p_1 \vec{p}_2 m_1 m_2 \right. \right. \right\rangle \right. \\ \left. + \sum_{S'M'_S} \int d\vec{q} \frac{\left\langle p_{\vec{\Lambda}p} S M_S \left| t^{\Lambda p \rightarrow \Lambda p}(\omega) \left| \vec{q} S' M'_S \right. \right. \right\rangle \left\langle p_{\vec{K}} \vec{q} S' M'_S \left| V_{pp \rightarrow K^+\Lambda p}^x \left| p_1 \vec{p}_2 m_1 m_2 \right. \right. \right\rangle}{\omega - E(q) + i\eta} \right] \quad (\text{A.2})$$

where ω is the energy corresponding to the asymptotic momentum $p_{\vec{\Lambda}p}$. The two terms in the square bracket correspond to the two diagrams in each of the Figs. 1a and 1b.

In the case of DKE (Fig. 1c), the amplitude $V_{pp \rightarrow K^+\Lambda p}^x$ reduces to the Lagrangian $\mathcal{L}_{pK^+\Lambda}$ and the Λ is produced off-shell with a momentum $\vec{q}_\Lambda = \vec{p}_1 - \vec{p}_K$. Since the observed Λ is on-shell, the first term in the square bracket of eq. (A.2) does not contribute. It is brought on-shell by its interaction with the other proton only, as given in the second term. The amplitude for DKE is thus given as,

$$T_{DKE} = i g_{K\Lambda N} \sqrt{\frac{E_1 + M_p}{2M_p}} \sqrt{\frac{E(q_\Lambda) + M_\Lambda}{2M_\Lambda}} \sum_{SM_S} \left\langle \frac{1}{2} \frac{1}{2} m_3 m_\Lambda \left| S M_S \right. \right\rangle \quad (\text{A.3}) \\ \times \sum_{S'M'_S m'_\Lambda} \frac{\left\langle p_{\vec{\Lambda}p} S M_S \left| t^{\Lambda p \rightarrow \Lambda p}(\omega) \left| \vec{q}_\Lambda S' M'_S \right. \right. \right\rangle \left\langle \frac{1}{2} \frac{1}{2} m_2 m'_\Lambda \left| S' M'_S \right. \right\rangle}{\omega - E(q_{\Lambda p})} \\ \times \left\langle m'_\Lambda \left| \vec{\sigma} \cdot \left(\frac{\vec{p}_1}{E_1 + M_p} - \frac{\vec{q}_\Lambda}{E(q_\Lambda) + M_\Lambda} \right) \left| m_1 \right. \right\rangle$$

where $\vec{q}_{\Lambda p}$ is the momentum of the proton and off-shell Λ in the Λp centre of mass system.

The matrix elements of the plane wave amplitude $V_{pp \rightarrow K^+\Lambda p}^K$ for kaon exchange are given as,

$$\begin{aligned}
\left\langle \vec{p}_K \vec{p}_3 \vec{p}_\Lambda m_3 m_\Lambda \left| V_{pp \rightarrow K+\Lambda p}^K \right| \vec{p}_1 \vec{p}_2 m_1 m_2 \right\rangle &= \frac{i g_{K\Lambda N}}{q_K^2 - M_K^2} \sqrt{\frac{E_2 + M_p}{2M_p}} \sqrt{\frac{E_\Lambda + M_\Lambda}{2M_\Lambda}} \quad (\text{A.4}) \\
\left\langle m_\Lambda \left| \vec{\sigma} \cdot \left(\frac{\vec{p}_2}{E_2 + M_p} - \frac{\vec{p}_\Lambda}{E_\Lambda + M_\Lambda} \right) \right| m_2 \right\rangle &\left[F_K(q_K^2) \right]^2 \\
&\times \left\langle \frac{1}{2} m_3 \vec{p}_K \vec{p}_3 \left| T_{K+p \rightarrow K+p} \right| \frac{1}{2} m_1 \vec{q}_K \vec{p}_1 \right\rangle
\end{aligned}$$

where M_p , M_Λ and M_K are the masses of the proton, Λ and kaon respectively, q_K is the four momentum carried by the exchanged kaon and the coupling constant $g_{K\Lambda N}=14.1$. The matrix elements $\langle |T_{K+p \rightarrow K+p}| \rangle$ are expanded in partial waves and expressed in terms of phase shifts [24]. The monopole form factor $F_K(q_K^2) = (\Lambda_K^2 - M_K^2)/(\Lambda_K^2 - q_K^2)$ (with $\Lambda_K=1.2$ GeV) takes care of the off-shell nature of the exchanged kaon.

In a similar way, the plane wave matrix elements for the pion exchange transition amplitude (Fig. 1b) are given as,

$$\begin{aligned}
\left\langle \vec{p}_K \vec{p}_3 \vec{p}_\Lambda m_3 m_\Lambda \left| V_{pp \rightarrow K+\Lambda p}^\pi \right| \vec{p}_1 \vec{p}_2 m_1 m_2 \right\rangle &= \frac{i g_{\pi NN}}{q_\pi^2 - M_\pi^2} \sqrt{\frac{E_2 + M_p}{2M_p}} \sqrt{\frac{E_3 + M_p}{2M_p}} \quad (\text{A.5}) \\
&\times \left\langle m_3 \left| \vec{\sigma} \cdot \left(\frac{\vec{p}_2}{E_2 + M_p} - \frac{\vec{p}_3}{E_3 + M_p} \right) \right| m_2 \right\rangle \left[F_\pi(q_\pi^2) \right]^2 \\
&\times \left\langle \frac{1}{2} m_\Lambda \vec{p}_K \vec{p}_\Lambda \left| T_{\pi^o p \rightarrow K+\Lambda} \right| \frac{1}{2} m_1 \vec{q}_\pi \vec{p}_1 \right\rangle
\end{aligned}$$

where q_π is the four momentum carried by the exchanged pion, M_π its mass, the coupling constant $g_{\pi NN}=13.3$ and $F_\pi(q_\pi^2)$ (with $\Lambda_\pi=1.3$ GeV) is the monopole form factor which takes care of the off-shell nature of the exchanged pion. The matrix elements $\langle |T_{\pi^o p \rightarrow K+\Lambda}| \rangle$ are also expanded in partial waves and are written using the amplitudes given in ref.[25]. We use the same form factors at both the upper and lower vertices in Figs. 1a and 1b for the kaon and pion exchange diagrams.

Coupled channel method for $t^{\Lambda p \rightarrow \Lambda p}$

Since the mass difference between the Λ and Σ hyperon is not large, the ΣN channel plays an important role in Λp scattering and should be treated in an exact coupled channel method. The matrix elements of the t-matrix in a coupled channel formalism can be written in matrix form as,

$$\begin{aligned}
\left\langle p_{\Lambda p}^{\vec{S} M_S} \mathbf{t}(\omega) \left| \vec{q} S' M'_S \right. \right\rangle &= \left\langle p_{\Lambda p}^{\vec{S} M_S} \left| \mathbf{V}(\omega) \right| \vec{q} S' M'_S \right\rangle \quad (\text{A.6}) \\
&+ \sum_{S'' M''_S} \int k^2 dk \left\langle p_{\Lambda p}^{\vec{S} M_S} \left| \mathbf{V}(\omega) \right| \vec{k} S'' M''_S \right\rangle \mathbf{G}_o(k, \omega) \left\langle \vec{k} S'' M''_S \left| \mathbf{t}(\omega) \right| \vec{q} S' M'_S \right\rangle
\end{aligned}$$

with,

$$\mathbf{t}(\omega) = \begin{pmatrix} t^{\Lambda p \rightarrow \Lambda p} & t^{\Lambda p \rightarrow \Sigma N} \\ t^{\Sigma N \rightarrow \Lambda p} & t^{\Sigma N \rightarrow \Sigma N} \end{pmatrix}, \quad \mathbf{V}(\omega) = \begin{pmatrix} V^{\Lambda p \rightarrow \Lambda p} & V^{\Lambda p \rightarrow \Sigma N} \\ V^{\Sigma N \rightarrow \Lambda p} & V^{\Sigma N \rightarrow \Sigma N} \end{pmatrix}$$

and,

$$\mathbf{G}_o(k, \omega) = \begin{pmatrix} \frac{1}{\omega - E_\Lambda(k) + i\epsilon} & 0 \\ 0 & \frac{1}{\omega - E_\Sigma(k) + i\epsilon} \end{pmatrix}$$

The matrix elements of $\mathbf{t}(\omega)$ can be expressed in terms of partial wave expansions as,

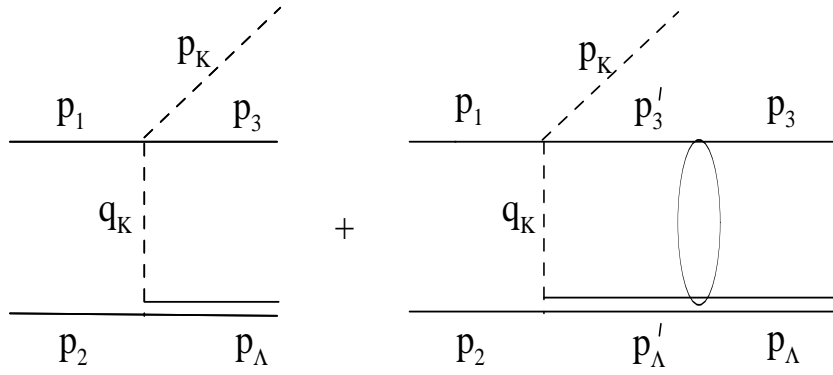
$$\begin{aligned} \left\langle p_{\Lambda p} \vec{S} M_S \left| \mathbf{t}(\omega) \right| \vec{q} S' M'_S \right\rangle &= \sum_{JM} \sum_{L' M'_L M'_S} Y_{LM_L}(p_{\Lambda p}) Y_{L' M'_L}^*(\hat{q}) \quad (\text{A.7}) \\ \left\langle L M_L S M_S \left| JM \right\rangle \left\langle L' M'_L S' M'_S \left| JM \right\rangle \left\langle JM(LS) p_{\Lambda p} \left| \mathbf{t}(\omega) \right| q(L' S') JM \right\rangle \end{aligned}$$

We evaluate the matrix elements of $t^{\Lambda p \rightarrow \Lambda p}(\omega)$ in eq.(A.2) numerically, using eqs.(A.6) and (A.7) and the available YN potentials $\mathbf{V}(\omega)$. The on-shell amplitudes evaluated using our t-matrix code are in good agreement with the values published in the original works of the Nijmegen and Jülich groups.

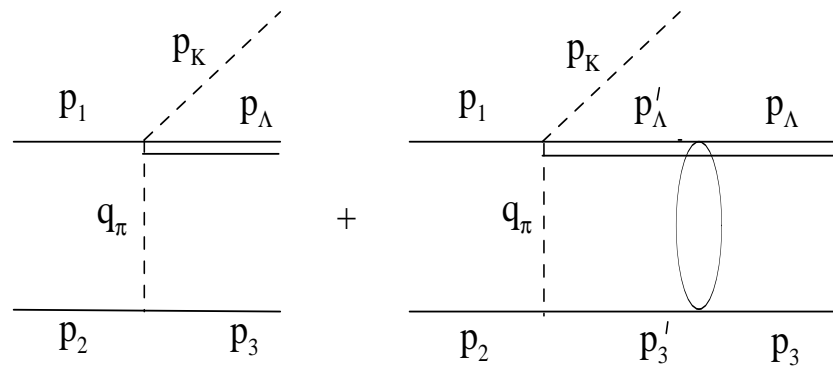
References

- [1] J. K. Ahn *et al.*, Nucl. Phys. **A648** (1999) 263.
- [2] G. Alexander *et al.*, Phys. Rev. **173** (1968) 1452; B. Sechi-Zorn, B. Kehoe, J. Twitty and R. A. Burnstein, Phys. Rev. **175** (1968) 1735; R. Engelman, H. Filthuth, V. Hepp and E. Kluge, Phys. Lett. **21** (1966) 587; F. Eisele, H. Filthuth, W. Föhlisch, V. Hepp and G. Zech, Phys. Lett. **B37** (1971) 204; V. Hepp and M. Schleich, Z. Phys. **214** (1968) 71; J. A. Kadyk *et al.*, Nucl. Phys. **B27** (1971) 13; J. M. Hauptmann, J. A. Kadyk and G. H. Trilling, Nucl. Phys. **B125** (1977) 29.
- [3] C. Pigot *et al.*, Nucl. Phys. **B249** (1985) 172; O. Braun *et al.*, Nucl. Phys. **B124** (1977) 45; T. H. Tan, Phys. Rev. Lett. **23** (1969) 395, Phys. Rev. **D7** (1972) 600; G. D'Agostini *et al.*, Phys. Lett. **B104** (1981) 330.
- [4] Siebert *et al.*, Nucl. Phys. **A567** (1994) 819.
- [5] R. Frascaria *et al.*, Nuovo Cimento **A102** (1989) 561.
- [6] J. T. Balewski *et al.*, Phys. Lett. **B388** (1996) 859.
- [7] R. Bilger *et al.*, Phys. Lett. **B420** (1998) 217; S. Sewerin *et al.*, Phys. Rev. Lett. **83** (1999) 682; J. T. Balewski *et al.*, Phys. Lett. **B420** (1998) 211.
- [8] A. Sibirtsev and W. Cassing, IFJ-1787-PH, nucl-th/9802019; A. Sibirtsev, Phys. Lett. **B359** (1995) 29.
- [9] K. Tsushima, A. Sibirtsev and A. W. Thomas, Phys. Lett. **B390** (1997) 29; A. Sibirtsev, K. Tsushima and A. W. Thomas, Phys. Lett. **B421** (1998) 59; R. Shyam, Phys. Rev. **C60** (1999) 55213.
- [10] J. M. Laget, Phys. Lett. **B259** (1991) 24.
- [11] Landolt - Börnstein, New Series, ed. H. Schopper, I/12 (1988).
- [12] Flaminio *et al.*, Compilation of cross sections, CERN-HERA
- [13] A. Deloff, Nucl. Phys. **A505** (1989) 583.
- [14] A. Parreño, A. Ramos, N. G. Kelkar and C. Bennhold, Phys. Rev. **C59** (1999) 2122.
- [15] P.M.M. Maessen, Th. A. Rijken and J.J. de Swart, Phys. Rev. **C40** (1989) 2226.
- [16] Th. A. Rijken, V. C. J. Stoks and Y. Yamamoto, Phys. Rev. **C59** (1999) 21.
- [17] M. M. Nagels, T. A. Rijken and J. J. de Swart, Phys. Rev. **D15** (1977) 2547; *ibid* Phys. Rev. **D20** (1979) 1633.
- [18] B. Holzenkamp, K. Holinde, and J. Speth, Nucl. Phys. **A500** (1989) 485; A. Reuber, K. Holinde and J. Speth, Nucl. Phys. **A570** (1994) 543.

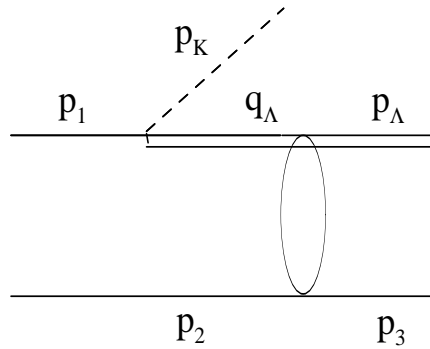
- [19] Y. Fujiwara, T. Fujita, C. Nakamoto and Y. Suzuki, Nucl. Phys. **A629** (1998) 190c; Y. Fujiwara, C. Nakamoto and Y. Suzuki, Phys. Rev. Lett. **76** (1996) 2242; *ibid* Prog. Theor. Phys. **94** (1995) 215; **94** (1995) 353.
- [20] Z. Y. Zhang *et al.*, Nucl. Phys. **A625** (1997) 59; Z. Y. Zhang, You-Wen Yu, Peng-Nian Shen and Lian-Rong Dai, Commun. Theor. Phys. **30** (1998) 213.
- [21] M. Oka, Nucl. Phys. **A629** (1998) 379c; *ibid* Prog. Theor. Phys. Suppl. **120** (1995) 95; M. Oka, Y. Tani, T. Inoue and K. Sasaki, nucl-th/981103. report 79-03 (1979).
- [22] Byckling and Kajantie, Particle Kinematics, Wiley-Interscience Publication (1973).
- [23] A. Reuber, K. Holinde, H. C. Kim and J. Speth, Nucl. Phys. **A608** (1996) 243.
- [24] G. Giacomelli *et al.*, Nucl. Phys. **B20** (1970) 301.
- [25] M. Sotona and J. Žofka, Prog. of Theor. Phys. **81** (1989) 160.
- [26] J. Haidenbauer, K. Holinde, K. Kilian, T. Sefzick and A. W. Thomas, Phys. Rev. **C52** (1995) 3496 .
- [27] A. Gasparian *et al.*, Phys. Lett. **B480** (2000) 273.
- [28] K. Miyagawa and H. Yamamura, Phys. Rev. **C60** (1999) 24003.
- [29] F. Balestra *et al.*, Phys. Rev. Lett. **83** (1999) 1534.



(a) kaon exchange



(b) pion exchange



(c) direct kaon emission

Figure 1: Diagrams for the $pp \rightarrow K^+\Lambda p$ reaction (a) kaon exchange (b) pion exchange (c) direct kaon emission. The ellipses indicate the final state interactions of the Λ and proton.

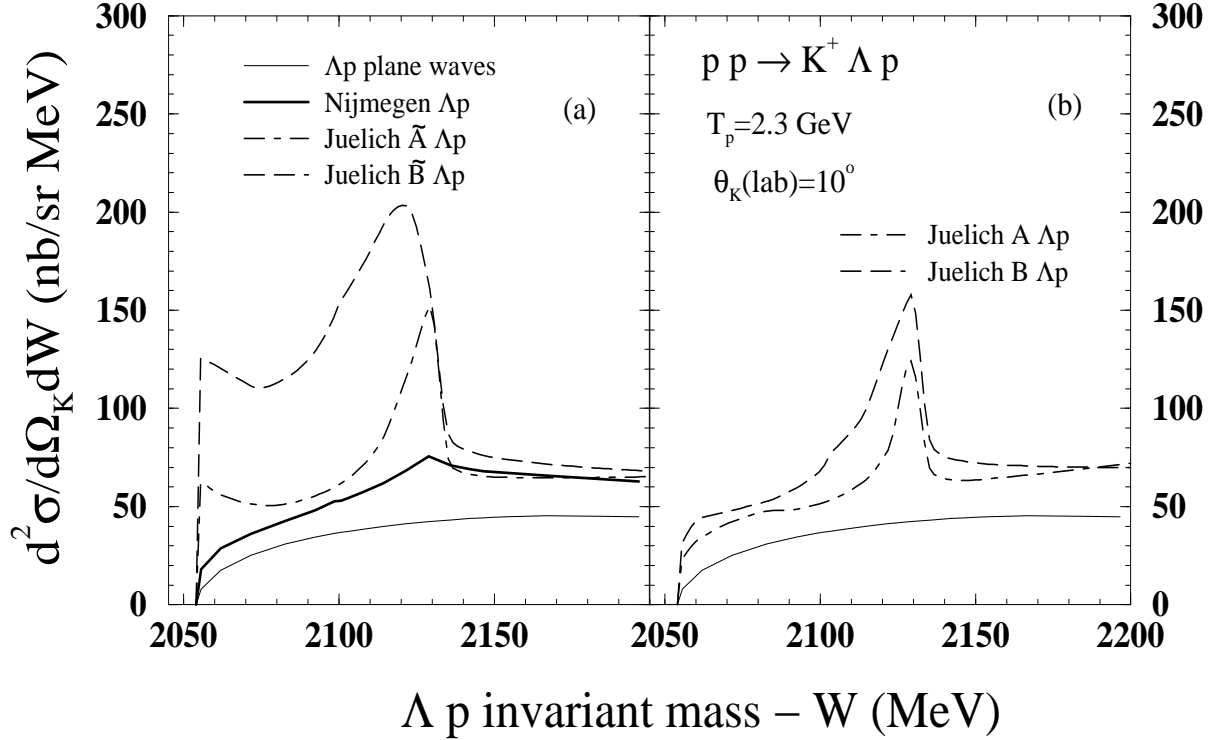


Figure 2: Λp invariant mass spectra at 2.3 GeV beam energy for the exclusive $pp \rightarrow K^+ \Lambda p$ reaction calculated using different potentials for the Λp final state interaction. (a) thick solid line uses the Nijmegen soft-core potential, dash-dotted and dashed curves are calculations using versions \tilde{A} and \tilde{B} respectively of the energy independent Jülich potential. (b) Calculations using energy dependent versions A (dash-dotted curve) and B (dashed curve) of the Jülich potential. The thin solid lines in (a) and (b) are the results using plane waves for the Λ and proton in the final state.

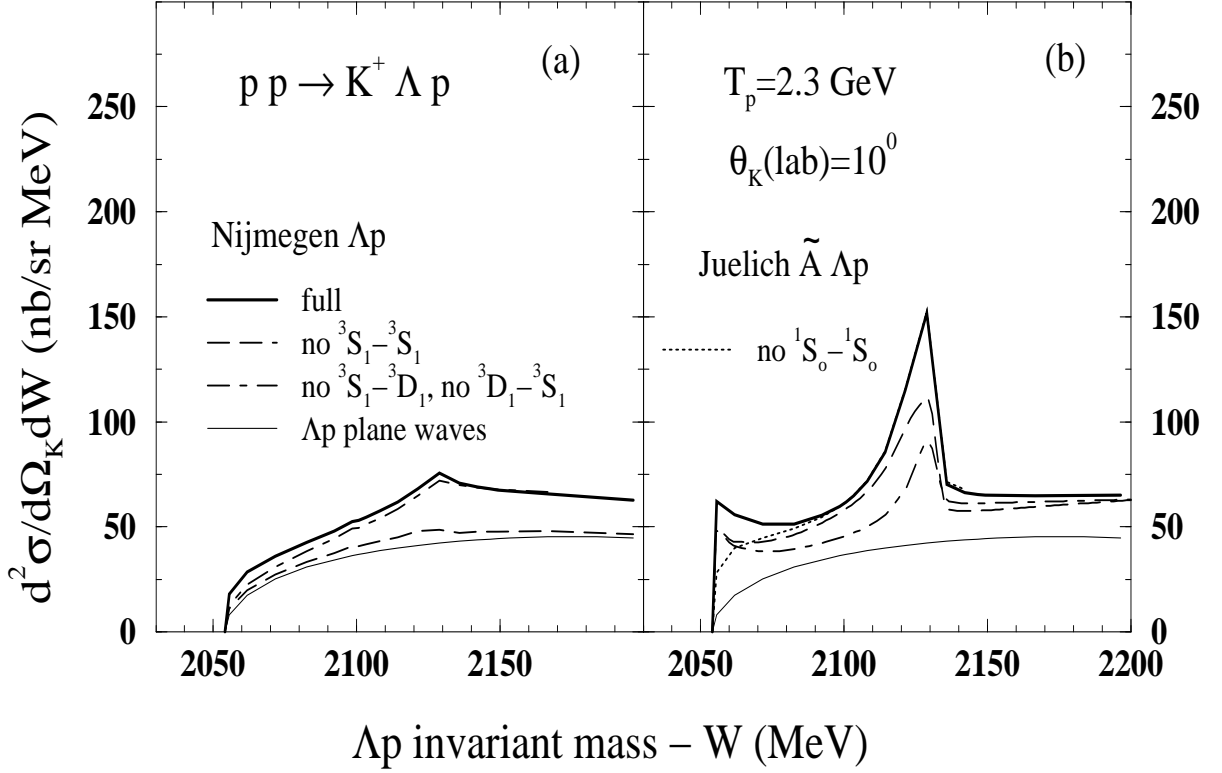


Figure 3: Contribution of the various channels of the Λp elastic scattering to the Λp invariant mass spectra for the $pp \rightarrow K^+ \Lambda p$ reaction. Thin solid lines are the cross sections obtained using plane waves for the final state Λ and proton. Dashed lines are the results obtained after removing the ${}^3S_1 - {}^3S_1$ channel from $\langle JM(LS)p_{\Lambda p} | t^{\Lambda p \rightarrow \Lambda p} | q(L'S') JM \rangle$. Dash-dotted lines are the results obtained by dropping the ${}^3S_1 - {}^3D_1$ and ${}^3D_1 - {}^3S_1$ channels and dotted lines are those after removing the ${}^1S_0 - {}^1S_0$ transition. Results are shown using two types of YN potentials (a) Nijmegen and (b) Jülich $\tilde{\Lambda}$.

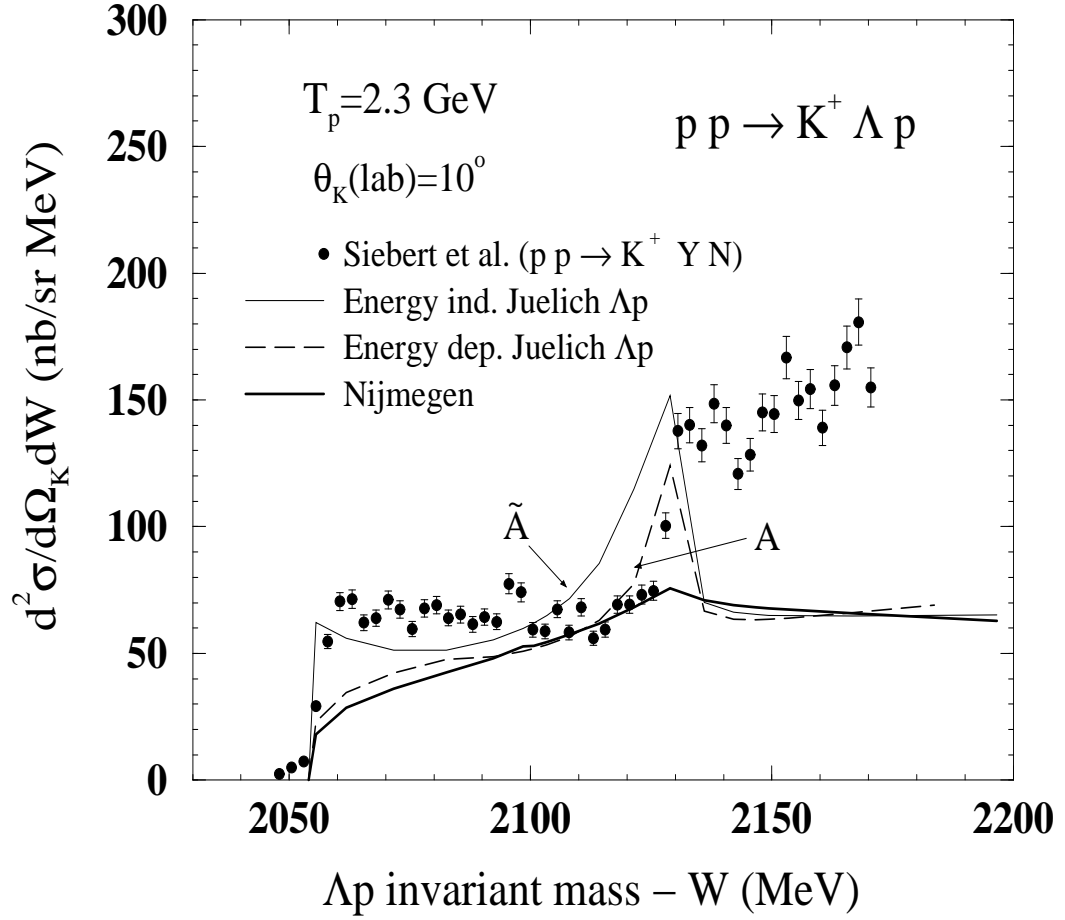


Figure 4: Comparison of calculated invariant Λp mass spectra for the $pp \rightarrow K^+ \Lambda p$ reaction with the available inclusive data on the $pp \rightarrow K^+ Y N$ reaction. The data are from ref. [4]. The thick solid line is the calculation using the Nijmegen soft-core Λp potential. The thin solid line and dashed line are respectively the results using energy independent and dependent versions of the Jülich potential A.

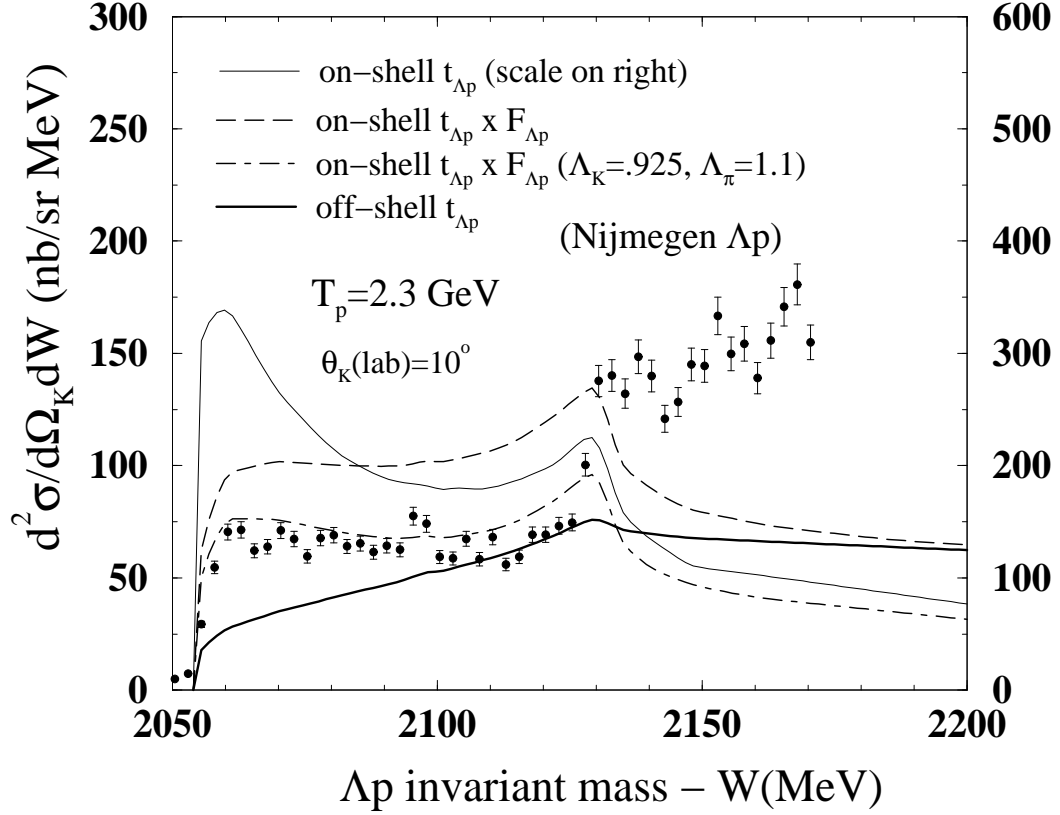


Figure 5: Effects of on-shell approximations of the final state Λp interaction on the Λp mass spectra for the $pp \rightarrow K^+ \Lambda p$ reaction. Calculations are done using the Nijmegen Λp potential. The thin solid line is the calculation (with scale given on the right) using on-shell matrix elements of the t -matrix for $\Lambda p \rightarrow \Lambda p$. Dashed curve is obtained by multiplying the on-shell matrix elements of $t^{\Lambda p \rightarrow \Lambda p}$ by a form factor $F_{\Lambda p}$ (scale on left). Dash-dotted curve is obtained by reducing the values of Λ_K and Λ_π in a calculation similar to that of the dashed curve. The thick solid line uses the off-shell matrix elements of $t^{\Lambda p \rightarrow \Lambda p}$ (as used throughout this work). The solid curves and the dashed curve show results using $\Lambda_K = 1.2$ and $\Lambda_\pi = 1.3$ GeV. The data is the same as in Fig. 4.

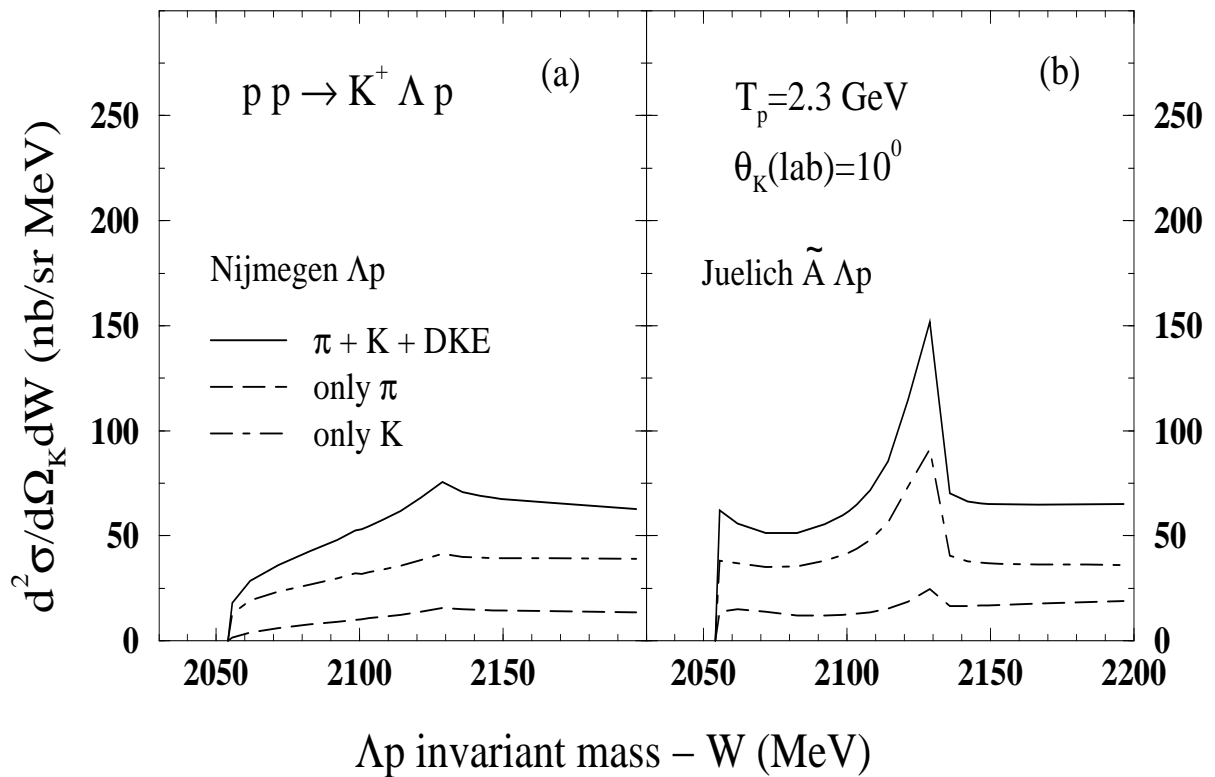


Figure 6: Contributions of the various meson exchange diagrams to the $pp \rightarrow K^+ \Lambda p$ reaction using (a) Nijmegen and (b) Jülich \tilde{A} potentials for Λp final state interaction. The solid curves are the calculations including all diagrams of Fig. 1. Dashed and dash-dotted curves are the cross sections using only pion and only kaon exchange mechanisms respectively.